Inorg. Chem. **2006**, *45*, 4743–4754

Charge Distribution in Chromium and Vanadium Catecholato Complexes: X-ray Absorption Spectroscopic and Computational Studies

Carsten Milsmann,[†,‡] Aviva Levina,[†] Hugh H. Harris,[†] Garry J. Foran,[§] Peter Turner,[†] and Peter A. Lay*[,†]

Centre for Heavy Metals Research and Centre for Structural Biology and Chemistry, School of Chemistry, The University of Sydney, Sydney NSW 2006, Australia, and Australian Nuclear Science and Technology Organization, PMB 1, Menai NSW 2234, Australia

Received March 4, 2006

Transition-metal complexes with redox-active catecholato ligands are of interest as models of bioinorganic systems and as potential molecular materials. This work expands our recent X-ray absorption spectroscopic (XAS) studies of Cr(V/IV/III) triscatecholato complexes (Levina, A.; Foran, G. J.; Pattison, D. I.; Lay, P. A. *Angew. Chem., Int. Ed.* **2004**, *43*, 462–465) to a Cr(III) monocatecholato complex, $[Cr(tren)(cat)]^+$ (tren = tris(2-aminoethyl)amine, cat = catecholato(2–)), and its oxidized analogue, as well as to a series of V(V/IV/III) triscatecholato complexes ($[VL_3]^{n-}$, where L = cat, 3,5-di-*tert*-butylcatecholato(2–), or tetrachlorocatecholato(2–), and n = 1–3). Various oxidation states of these complexes in solutions were generated by bulk electrolysis directly in the XAS cell. Increases in the edge energies and pre-edge absorbance intensities in XANES spectra, as well as decreases in the average M–O bond lengths (M = Cr or V) revealed by XAFS data analyses, are consistent with predominantly metal-based oxidations in both the Cr(V/IV/III) and V(V/IV/III) triscatecholato series, but the degree of electron delocalization between the metal ion and the ligands was higher in the case of Cr complexes. By contrast, oxidation of $[Cr^{III}(tren)(cat)]^+$ was mainly ligand-based and led to $[Cr^{III}(tren)(sq)]^{2+}$ (sq = semiquinonato(–)), as shown by the absence of significant changes in the pre-edge and edge features and by an increase in the average Cr–O bond length. The observed differences in electron-density distribution in various oxidation states of Cr and V mono- and triscatecholato complexes have been discussed on the basis of the results of density functional calculations. A crystal and molecular structure of $(Et_3NH)_2[V^{IV}(cat)_3]$ has been determined at 25 K and the same complex with an acetonitrile of crystallization at 150 K.

Introduction

Transition-metal complexes of redox-active ligands, including catechols (1,2-dihydroxybenzene and its derivatives), have attracted considerable attention both as challenging models for theoretical studies[1−3] and as potential conductive or magnetic molecular materials[4] or biologically active compounds.[5−7] For instance, Cr complexes of catecholamines have been implicated as possible reactive species in Cr(VI)-induced genotoxicity and carcinogenicity,[8] and V complexes with catechol-like ligands have been detected in the blood of some marine invertebrates.[9]

* To whom correspondence should be addressed. E-mail: p.lay@chem.usyd.edu.au.

† The University of Sydney.

‡ Fachbereich chemie, Philipps-Universität, Marburg, Hans-Meerwein-Strasse, D-35032 Marburg, Germany.

§ Australian Nuclear Science and Technology Organization.

(1) (a) Pierpont, C. G. *Coord. Chem. Rev.* **2001**, *216−217*, 99−125. (b) Pierpont, C. G. *Coord. Chem. Rev.* **2001**, *219−221*, 415−433 and references therein.

(2) Rodriguez, J. H.; Wheeler, D. E.; McCusker, J. K. *J. Am. Chem. Soc.* **1998**, *120*, 12051−12068.

(3) Gordon, D. J.; Fenske, R. F. *Inorg. Chem.* **1982**, *21*, 2908−2915.

(4) (a) Chang, H.-C.; Miyasaka, H.; Kitagawa, S. *Inorg. Chem.* **2001**, *40*, 146−156. (b) Chang, H.-C.; Kitagawa, S. *Angew. Chem., Int. Ed.* **2002**, *41*, 130−133.

(5) (a) Isied, S. S.; Kuo, G.; Raymond, K. N. *J. Am. Chem. Soc.* **1976**, *98*, 1763−1767. (b) Raymond, K. N.; Isied, S. S.; Brown, L. D.; Fronczek, F. R.; Nibert, J. H. *J. Am. Chem. Soc.* **1976**, *98*, 1767−1774.

(6) Farmer, P. J.; Gidanian, S.; Shahandeh, B.; Di Bilio, A. J.; Tohidian, N.; Meyskens, F. L., Jr. *Pigm. Cell Res.* **2003**, *16*, 273−279.

(7) Humphries, W. R. (Rowett Research Services Ltd., U.K.). World Patent Application 9909050, 1999; *Chem Abstr*. **1999**, *130*, 205114.

(8) Pattison, D. I.; Davies, M. J.; Levina, A.; Dixon, N. E.; Lay, P. A. *Chem. Res. Toxicol.* **2001**, *14*, 500−510.

(9) (a) Frank, P.; Hodgson, K. O. *Inorg. Chem.* **2000**, *39*, 6018−6027. (b) Frank, P.; Robinson, W. E.; Kustin, K.; Hodgson, K. O. *J. Inorg. Biochem.* **2001**, *86*, 635−648.

10.1021/ic0603611 CCC: $33.50
Published on Web 05/17/2006

Assignment of the spectroscopic oxidation states in complexes in which both the metal ion and the ligands are redox-active is problematic,[3,10] as shown by the recent debate over the Cr oxidation states in triscatecholato complexes.[11,12] Such assignments usually rely on small changes in the O−C and C−C bond lengths in the ligands, as detected by X-ray crystallography.[1] The recent application of electrochemical X-ray absorption spectroscopy (XAS) provided several new opportunities for the study of electron-transfer reactions in such complexes for the following reasons:[13,14] (i) unstable redox states were generated in solutions directly in the XAS cell, so that the structures of several members of a redox series could be examined in the same medium; (ii) a required oxidation state of the complex could be maintained throughout the XAS data acquisition by continuous application of an electrochemical potential, which removes the common problem of photoreduction of the sample; (iii) a direct measure of the oxidation state of the metal ion was provided by X-ray absorption near-edge structure (XANES) spectroscopy; and (iv) multiple-scattering (MS) analysis of X-ray absorption fine structure (XAFS) spectra provides both a good indication of the integrity and purity of the sample and precise values of the metal−ligand bond lengths (within ∼0.005 Å). The latter point is particularly important, because one of the best indications of an increase in metal oxidation state in a series of complexes with the same ligands is a decrease in average metal−ligand bond lengths due to increased electron-withdrawal ability of the metal ion.[15] The metal−ligand bond lengths determined by MS fittings of XAFS spectra collected in solutions are often more informative than those determined by X-ray crystallography because of the elimination of crystal packing forces.[14]

Electrochemical XAS studies[13] have shown (contrary to a dominant opinion)[1,12] that sequential one-electron oxidations of the $[Cr^{III}(cat)_3]^{3-}$ complex (cat = catecholato(2−)) lead to increases in the effective (spectroscopic) oxidation states of the Cr ion, so that the products can be assigned as the $[Cr^{IV}(cat)_3]^{2-}$ and $[Cr^{V}(cat)_3]^{-}$ complexes with a strong electron delocalization between the metal ion and the ligands. In this work, such studies have been expanded to a series of V(V/IV/III) triscatecholato complexes, in which the redox reactions are indisputably metal-based (as determined from the crystallographic data).[12] It was, therefore, instructive to compare the changes in XANES and XAFS spectra in the V(V/IV/III) and Cr(V/IV/III) redox series. On the other hand, recent X-ray crystallographic and computational studies[2,16] of a Cr(III) monocatecholato complex, $[Cr(tren)(3,6\text{-dtbc})]^{+}$ (tren = tris(2-aminoethyl)amine, 3,6-dtbc = 3,6-di-*tert*-butylcatecholato(2−)), and its oxidation product provided strong evidence that one-electron oxidation of this compound is ligand-based and leads to a relatively stable Cr(III) semiquinonato complex. In this work, redox reactions of a closely related complex, $[Cr^{III}(tren)(cat)]^{+}$, were studied by electrochemical XAS in comparison with those of $[Cr^{III}(cat)_3]^{3-}$.[13]

Previous computational studies on Cr and V catecholato complexes include molecular orbital (MO) calculations for the $[M(cat)_3]^{n-}$ series (M = Cr or V; $n = 0-3$)[3] and density functional theory (DFT) calculations for $[Cr(tren)(3,6\text{-dtbc})]^{+}$ and its oxidized analogue.[2] In this work, the use of the DFT technique was expanded to Cr and V triscatecholato complexes, and the results were used to help in the interpretation of electrochemical XAS data.

Experimental Section

General Techniques. Commercial reagents of analytical or higher purity (from Aldrich or Merck) and HPLC grade solvents (from Aldrich) were used without further purification. All synthetic and analytical procedures involving solutions of catechols and their complexes were performed under an atmosphere of high purity Ar (BOC gases), using standard Schlenk techniques. Solid catecholato complexes were kept for several months at ∼22 °C in tightly closed Ar-flushed vials; brief handling of these compounds under an ambient atmosphere did not result in significant decomposition of the samples.

Elemental analyses (C, H, N) were carried out by the Australian National University Microanalytical Unit. Determinations of metal contents in the complexes (after their digestion with 69% HNO_3) were performed by C_2H_2/air flame atomic absorption spectroscopy (AAS) for Cr and by graphite furnace AAS for V, using Varian SpecAA-800 or SpecAA-20 spectrometers, respectively, calibrated with Cr(III) or V(IV) standard solutions (Aldrich). Solid-state Fourier transform infrared (FTIR) spectra were recorded using the diffuse reflectance technique (for the mixtures with KBr) on a Bio-Rad FTS-40 spectrometer. Electronic absorption (UV−vis) spectra in solutions were recorded on a Hewlett−Packard HP8452A diode-array spectrometer or a Varian Cary-5E spectrometer.

Solution EPR spectra (X-band, 22 °C) were acquired on a Bruker EMX spectrometer, using a Wilmad quartz flat cell. Calibrations of the magnetic field and the microwave frequency were performed with an EMX 035 NMR gaussmeter and an EMX 048T microwave bridge controller, respectively. Typical instrumental settings were as follows: center field, 3480 G; sweep width, 1000 G; resolution, 1024 points; microwave power, 2.0 mW; microwave frequency, ∼9.67 GHz; modulation frequency, 100 kHz; modulation amplitude, 5.0 G; time constant, 20.48 ms; receiver gain, 1×10^4; and number of scans, 5. The EPR spectra were processed with WinEPR software;[17] second-order corrections were applied in the determination of the g_{iso} and A_{iso} values.

Electrospray mass spectrometry (ESMS) was performed on a Finnigan LCQ spectrometer, using the following experimental settings: sheath gas (N_2) pressure, 60 psi; spray voltage, 4.0 kV; capillary temperature, 200 °C; cone voltage, 25 V; tube lens offset, 20 V; *m*/*z* range, 100−2000 (both in positive- and negative-ion modes; no significant signals were detected at $m/z > 1000$). Variations in the capillary temperature (150−220 °C) and cone voltage (5−40 V) did not cause qualitative changes in the spectra. Analyzed solutions (5 μL, ∼1 mM Cr or V) in MeOH or MeCN

(10) Chaudhuri, P.; Wieghardt, K. *Prog. Inorg. Chem.* **2001**, *50*, 151−216.
(11) Pattison, D. I., Levina, A.; Davies, M. J.; Lay, P. A. *Inorg. Chem.* **2001**, *40*, 214−217.
(12) Pierpont, C. G. *Inorg. Chem.* **2001**, *40*, 5727−5728.
(13) Levina, A.; Foran, G. J.; Pattison, D. I.; Lay, P. A. *Angew. Chem., Int. Ed.* **2004**, *43*, 462−465.
(14) Levina, A.; Armstrong, R. S.; Lay, P. A. *Coord. Chem. Rev.* **2005**, *249*, 141−160.
(15) Wood, R. M.; Abboud, K. A.; Palenik, R. C.; Palenik, G. J. *Inorg. Chem.* **2000**, *39*, 2065−2068.
(16) Wheeler, D. E.; McCusker, J. K. *Inorg. Chem.* **1998**, *37*, 2296−2307.
(17) *WinEPR*, version 960801; Bruker-Franzen Analytic: Bremen, Germany, 1996.

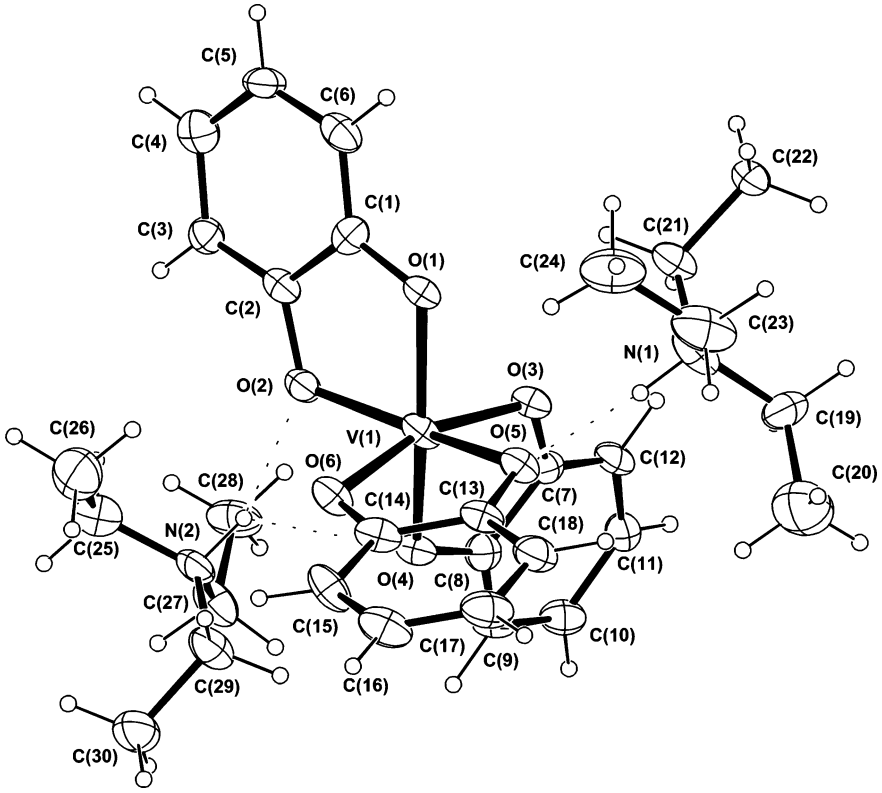

Figure 1. An ORTEP[29] depiction of $(Et_3NH)_2[V^{IV}(cat)_3]$ at 25 K, showing 50% probability level displacement ellipsoids. Details of the refined model are given in Table S1 of the Supporting Information and in the CIF file. The V−O(*n*) bond lengths are 1.935(3), 1.951(3), 1.939(3), 1.951(3), 1.963(3), and 1.931(3) Å, respectively, for $n = 1-6$. The structure was similar for $(Et_3NH)_2[V^{IV}(cat)_3]\cdot CH_3CN$ at 150 K (obtained on the same crystal prior to the 25 K structure), except for the presence of a solvent of crystallization; the V−O(*n*) bond lengths are 1.934(2), 1.962(2), 1.941(2), 1.938(2), 1.966(2), and 1.928(2) Å, respectively, for $n = 1-6$.

were injected into a flow of 1:1 v/v H_2O:MeOH (flow rate, 0.20 mL min^{-1}). The acquired ESMS data were averaged over 10 scans (scan time, 10 ms) and analyzed with IsoPro software.[18]

Cyclic voltammetry (CV) experiments were performed using a Bioanalytical Systems BAS 100B Electrochemical Analyzer (scan rate, 100 mV s^{-1}; 100% *iR* compensation) with a glassy carbon working electrode (diameter, 3.0 mm), a Ag/AgCl reference electrode filled with 3.0 M aqueous NaCl, and Pt wire as an auxiliary electrode. Bulk electrolysis was performed in a glass cell with a working electrode made of reticulated vitreous carbon (45 PPI, The Electrosynthesis Co., East Amherst, NY), a Ag/AgCl reference electrode, and Pt mesh as an auxiliary electrode, using a PAR 273A potentiostat/galvanostat (Princeton Applied Research, Princeton, NJ) for maintaining the required potential and coulometric measurements. For the electrochemical experiments, the complexes (10 mM) were dissolved in anhydrous *N*,*N*-dimethylformamide (DMF) or MeCN, both containing $(^nBu_4N)BF_4$ (0.10 M) as the supporting electrolyte. The ferrocenium/ferrocene couple (Fc^+/Fc) was used as an internal standard for the potential calibration in the CV experiments. Samples of the reaction solutions, taken during the bulk electrolysis experiments, were diluted 100-fold with Ar-saturated solvents for UV−vis spectroscopy or used undiluted for EPR spectroscopy.

Syntheses and X-ray Crystallography of Catecholato Complexes. The complexes, $[Cr^{III}(tren)(cat)]Cl$, $(Et_3NH)_2[V^{IV}(cat)_3]$, $(Et_3NH)[V^{V}(dtbc)_3]$ (dtbc = 3,5-di-*tert*-butylcatecholato(2−)), and $(Et_3NH)_2[V^{IV}(tcc)_3]$ (tcc = tetrachlorocatecholato(2−)), were synthesized by modifications of the published procedures.[16,19,20] Details of syntheses and characterizations of the complexes (including elemental analyses, ESMS, FTIR, and EPR spectroscopic data) are given in the Supporting Information.

An X-ray quality crystal of $(Et_3NH)_2[V^{IV}(cat)_3]\cdot CH_3CN$ was grown from a saturated solution of the complex in MeCN (4 °C, under Ar). X-ray diffraction data were collected on the same crystal at 150 ± 2 K and subsequently at 25 ± 2 K (the CH_3CN of crystallization was lost from the crystal between the two determinations) and were analyzed using standard procedures[21−29] (see the Supporting Information for details). The crystal data and refinement details are summarized in Table S1 of the Supporting Information;

(18) Senko, M. *IsoPro 3.0*; Sunnyvale, CA, 1998.

(19) Zipp, S. G.; Madan, S. K. *Inorg. Chem.* **1976**, *15*, 587−593.
(20) Cooper, S. R.; Bai Koh, Y.; Raymond, K. N. *J. Am. Chem. Soc.* **1982**, *104*, 5092−5102.
(21) *SMART, SAINT, and XPREP. Area Detector Control and Data Integration and Reduction Software*; Bruker Analytical X-ray Instruments Inc.: Madison, WI, 1995.
(22) *teXsan for Windows: Single Crystal Structure Analysis Software*; Molecular Structure Corporation: The Woodlands, TX, 1997.
(23) Farrugia, L. J. *J. Appl. Cryst.* **1999**, *32*, 837−838.
(24) Hall, S. R.; du Boulay, D. J.; Olthof-Hazekamp, R. *Xtal 3.6 System*; University of Western Australia: Perth, Australia, 1999.
(25) Coppens, P.; Leiserowitz, L.; Rabinovich, D. *Acta Crystallogr.* **1965**, *18*, 1035−1038.
(26) Altomare, A.; Burla, M. C.; Camalli, M.; Cascarano, G. L.; Giacovazzo, C.; Guagliardi, A.; Moliterni, A. G. G.; Polidori, G.; Spagna, R. *J. Appl. Cryst.* **1998**, *32*, 115−119.
(27) Sheldrick, G. M. *SHELXL97*: *Program for Crystal Structure Refinement*; University of Göttingen: Göttingen, Germany, 1997.
(28) (a) Flack, H. D. *Acta Crystallogr., Sect. A* **1983**, *39*, 876−881. (b) Bernardinelli, G.; Flack, H. D. *Acta Crystallogr., Sect. A* **1985**, *41*, 500−511. (c) Flack, H. D.; Bernardinelli, G. *Acta Crystallogr., Sect. A* **1999**, *55*, 908−915. (d) Flack, H. D.; Bernardinelli, G. *J. Appl. Cryst.* **2000**, *33*, 1143−1148.
(29) Johnson, C. K. *ORTEPII*; Report ORNL-5138; Oak Ridge National Laboratory: Oak Ridge, TN, 1976.

an ORTEP[29] depiction of the complex at 25 K is shown in Figure 1, and details of the optimized structures of $(Et_3NH)_2[V^{IV}(cat)_3]$ (25 K) and $(Et_3NH)_2[V^{IV}(cat)_3]\cdot CH_3CN$ (150 K) are attached as CIF files.

X-ray Absorption Spectroscopy (XAS) and Data Analysis. Chromium and vanadium K-edge spectra (in fluorescence detection mode) were recorded at the Australian National Beamline Facility (ANBF; beamline 20B at the Photon Factory, Tsukuba, Japan). The beamline parameters were as follows: beam energy, 2.5 eV; maximal beam current, 400 mA; light source, bending magnet; monochromator crystal, channel-cut Si[111] (nonfocusing, detuned by 50%); and detector, 10-element Ge array (Canberra). For all samples, 3−7 scans (scan time, 40−60 min) were taken at the following energy ranges: pre-edge region, 5770−5970 eV for Cr or 5250−5450 eV for V (10 eV steps); XANES region, 5970−6050 eV for Cr or 5450−5520 eV for V (0.25 eV steps); and XAFS region, 6050−7000 eV for Cr or 5520−6400 eV for V (0.05 $Å^{-1}$ steps in *k*-space). Energy calibration was performed by using a stainless steel foil (containing both Cr and V) as an internal standard (the first inflection points on the edges of Cr(0) or V(0) were assigned to 5989.0 or 5465.0 eV, respectively).[30] Bulk electrolysis of the reaction solutions for the in situ electrochemical XAS (at 22 °C) was performed as described in General Techniques, using a PAR 273A potentiostat and a specially constructed Teflon electrochemical cell (10 mL) with a Kapton film window.[13,31] At each applied potential, the electrolysis was allowed to proceed to completion (determined from the drop in the cell current to <5% of the initial value) before the XAS data collection was started, and the potential was maintained throughout the data collection. For solid-state XAS of reference vanadium compounds (22 °C), samples of $VOSO_4\cdot 5H_2O$ or $NaVO_3$ were mixed with boron nitride (BN, ∼1:20 w/w) and pressed into 0.5-mm pellets supported in an Al spacer between two 63.5 μm Kapton tape windows.

Averages, background subtraction, and calculations of theoretical XAFS spectra for Cr and V catecholato complexes were performed using the XFIT software package,[32] including FEFF 4.06[33] and FEFF 6.01[34] algorithms (for single- and multiple-scattering models, respectively), as described previously.[13,14,35] Starting coordinates for the multiple-scattering (MS) XAFS calculations were obtained from the crystal structures of $[Cr^{III}(tren)(3,6\text{-dtbc})](ClO_4)^2$ and $(Et_3NH)_2[V^{IV}(cat)_3]$ (this work). Details of the applied MS XAFS models are given in the Supporting Information. The three catecholato ligands in V triscatecholato complexes were set to be equal by application of D_3 symmetry and Debye−Waller factor constraints, which significantly reduced the number of varied parameters.[11,13,40] In all the models, the equivalent bond lengths and angles were restrained to be equal (within 0.02 Å or 2−5°, respectively). The benzene rings were restrained to be planar (within 0.1°), and the bond lengths and angles within the rings were restrained to 1.39 ± 0.02 Å and 120 ± 2°, respectively. The determinancies (N_i/p, where N_i is the number of independent observations and p is the number of varied parameters) of the models were estimated by the method of Binsted et al.,[39] taking into account the applied restraints and constraints. Overdetermined models ($N_i/p \geq 1.2$) were used in XAFS calculations, which allowed meaningful solutions to be obtained.[14,39] Fitting of the models to the experimental XAFS data was performed by a Levenberg−Marquardt algorithm within the XFIT software,[32] and convergence was typically achieved after 200−300 iterations. The random errors in the estimated XAFS parameters, arising from the noise in the data, were determined by Monte Carlo analysis within the XFIT software.[32]

Chart 1. Structures of the Synthesized Cr and V Catecholato Complexes

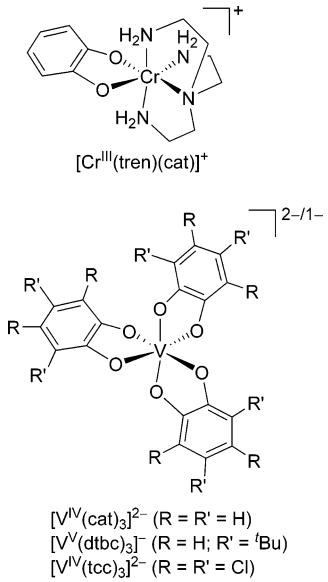

$[Cr^{III}(tren)(cat)]^+$

$[V^{IV}(cat)_3]^{2-}$ (R = R' = H)
$[V^{V}(dtbc)_3]^{-}$ (R = H; R' = ^{t}Bu)
$[V^{IV}(tcc)_3]^{2-}$ (R = R' = Cl)

Density Functional Calculations. Density functional theory molecular modeling used the program Dmol[3] Materials Studio, version 2.2.[36] The Becke exchange[37] and Perdew correlation[38] functionals (BP) were used to calculate both the potential during the SCF and the energy. Double numerical basis sets (DNP) included polarization functions for all atoms. Calculations were spin-unrestricted, and all electrons were considered as interacting. No symmetry constraints were applied, and geometries were optimized to an energy tolerance of 2.0×10^{-5} Ha. Starting structures were based on X-ray crystallographic coordinates from $K_3[Cr^{III}(cat)_3]$[5b] and $[Cr^{III}(tren)(3,6\text{-dtbc})](PF_6)$.[2] Mulliken population analyses were performed as implemented in the DMol[3] code.

Results

Syntheses, Characterization, and Electrochemistry of Cr and V Catecholato Complexes. A new complex, $[Cr^{III}(tren)(cat)]^+$ (see Chart 1), was synthesized by a ligand-exchange reaction of $catH_2$ with $[Cr^{III}(tren)Cl_2]^+$ (in a 1:1 molar ratio; see the Supporting Information). The use of $[Cr^{III}(tren)(cat)]^+$ instead of $[Cr^{III}(tren)(3,6\text{-dtbc})]^+$ did not require the synthesis of 3,6-dtbc,[16] and the product was more air-stable, which facilitated its purification and handling. Ligand-exchange reactions of catechols with $[V^{IV}O(acac)_2]$ (in a 4:1 molar ratio; see the Supporting Information) were

(30) *X-ray Data Booklet*; Lawrence Berkeley National Laboratory, University of California: Berkeley, CA, 2001.
(31) Barnard, P. J. Ph.D. Thesis, The University of Sydney, 2002.
(32) (a) Ellis, P. J.; Freeman, H. C. *J. Synchrotron Radiat.* **1995**, *2*, 190−195. (b) *XFIT for Windows95*; Australian Synchrotron Research Program: Sydney, Australia, 1996.
(33) Mustre de Leon, J.; Rehr, J. J.; Zabinsky, S. I.; Albers, R. C. *Phys. Rev. B.* **1991**, *44*, 4146−4156.
(34) Rehr, J. J.; Albers, R. C.; Zabinsky, S. I. *Phys. Rev. Lett.* **1992**, *69*, 3397−3400.
(35) Levina, A.; Codd, R.; Foran, G. J.; Hambley, T. W.; Maschmeyer, T.; Masters, A. F.; Lay, P. A. *Inorg. Chem.* **2004**, *43*, 1046−1055.
(36) (a) Delley, B. *J. Chem. Phys.* **1990**, *92*, 508−517. (b) Delley, B. *J. Chem. Phys*. **2000**, *113*, 7756−7764.
(37) Becke, A. D. *J. Chem. Phys.* **1988**, *88*, 2547−2553.
(38) Perdew, J. P.; Wang, Y. *Phys. Rev. B* **1992**, *45*, 13244−13249.
(39) Binsted, N.; Strange, R. W.; Hasnain, S. S. *Biochemistry* **1992**, *31*, 12117−12125.
(40) (a) Gaskell, S. J. *J. Mass Spectrom.* **1997**, *32*, 677−688. (b) Cole, R. B. *J. Mass Spectrom.* **2000**, *35*, 763−772.

applied to the syntheses of a series of V triscatecholato complexes (see Chart 1), including $[V^{IV}(cat)_3]^{2-}$ (which was described previously),[20] $[V^{IV}(tcc)]^{2-}$, and $[V^{V}(dtbc)_3]^{-}$. Oxidation of V(IV) to V(V) by trace O_2 occurred in the latter case, because of the low redox potential of the $[V^{V/IV}(dtbc)_3]^{-/2-}$ couple (see below).

The purity of $[Cr^{III}(tren)(cat)]^{+}$ was confirmed by ESMS (MeOH solution), which showed only the parent ion and its Cl^{-} adducts (see the Supporting Information, Figure S1 and Table S2). Mass spectra of $[V^{IV}(cat)_3]^{2-}$, $[V^{V}(dtbc)_3]^{-}$, and $[V^{IV}(tcc)]^{2-}$ (in MeCN solutions) showed signals due to the parent ions, as well as those due to their electrochemical reduction and cleavage reactions under the ESMS conditions[40] (particularly for the $[V^{IV}(cat)_3]^{2-}$ ion; see the Supporting Information, Figure S2 and Table S2). The UV−vis spectra of the complexes and the EPR spectra of the two V(IV) complexes were consistent with those reported in the literature (see λ_{max}, ϵ_{max}, g_{iso}, and A_{iso} values in the Supporting Information).[16,20] In the FTIR spectra of V(V/IV) triscatecholato complexes, the broad signals at ~3200 cm^{-1} due to ν_{O-H} in the corresponding catechols were absent (see the Supporting Information, Figure S3). The absence of a characteristic V═O stretching vibration at 937 cm^{-1} due to $[VO(acac)_2]$ (see the Supporting Information, Figure S3) also supported the purity of these complexes. Finally, the structures of $(Et_3NH)_2[V^{IV}(cat)_3]\cdot CH_3CN$ and $(Et_3NH)_2[V^{IV}(cat)_3]$ were confirmed by X-ray crystallography on the same crystal at 150 and 25 K, respectively (Figure 1 and the Supporting Information, Table S1 and CIF files), to compare with the structure of $(Et_3NH)_2[V^{IV}(cat)_3]\cdot CH_3CN$ determined previously at ~295 K,[20] although the space group was the same in all cases. The low-temperature structural determination was also undertaken to determine whether the V−O bond lengths increased with a reduction in temperature, as was observed for the Cr complexes,[13] but no increases were apparent (1.945 Å at 25 and 150 K, vs 1.942 Å at 295 K).[20] The results of elemental analyses for a bulk sample of $(Et_3NH)_2[V^{IV}(cat)_3]$ were also consistent with the absence of a solvent of crystallization.

The reversible one-electron oxidation of $[Cr^{III}(tren)(cat)]^{+}$, observed in the CV (Figure 2a and Table 1), was similar to that described previously for $[Cr^{III}(tren)(3,6\text{-dtbc})]^{+}$.[16] The CV results for the V triscatecholato complexes (Figure 2b−d and Table 1) showed quasireversible V(V/IV) couples for $[V^{IV}(cat)_3]^{2-}$ and $[V^{V}(dtbc)_3]^{-}$ (consistent with the literature data)[20,41] and a quasireversible V(IV/III) couple for $[V^{IV}(tcc)_3]^{2-}$, whereas the reductions of $[V^{IV}(cat)_3]^{2-}$ and $[V^{IV}(dtbc)_3]^{2-}$ and the oxidation of $[V^{IV}(tcc)_3]^{2-}$ were irreversible (Figure 2). The differences in the redox properties of various V−catecholato complexes are consistent with the electron-donating or electron-withdrawal properties of the *tert*-butyl or chloro substituents, respectively, in the catecholato ligands.[20,41] The $E_{1/2}$ values for all the reversible or quasireversible redox couples (both vs Ag/AgCl and vs Fc^{+}/Fc), including those reported previously for Cr triscatecholato complexes,[13] are listed in Table 1.

(41) Cass, M. E.; Gordon, N. R.; Pierpont, C. G. *Inorg. Chem.* **1986**, *25*, 3962−3967.

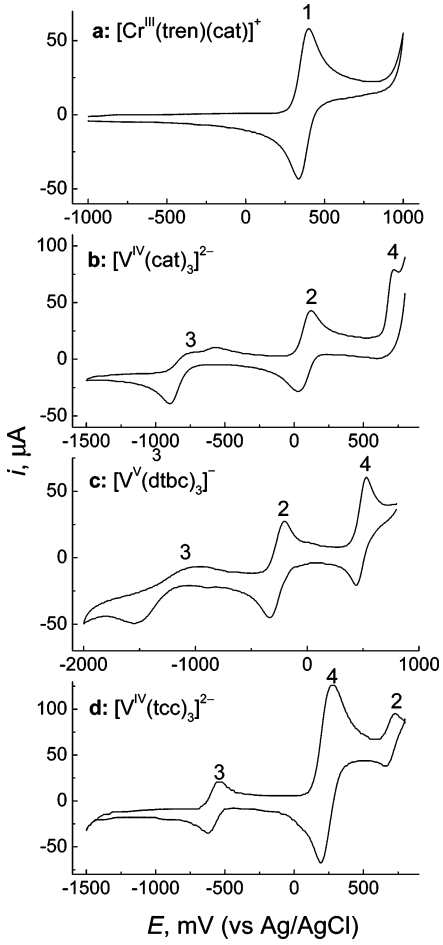

Figure 2. Typical cyclic voltammograms of Cr or V catecholato complexes (10 mM) in DMF (a) or MeCN (b−d) solutions in the presence of 0.10 M $(^nBu_4N)BF_4$ and the corresponding catechols (20 mM, b−d only) at 22 °C, 100 mV s^{-1} scan rate, 100% *iR* compensation. Designations of the signals: 1, $[Cr^{III}(tren)(sq)]^{2+}/[Cr^{III}(tren)(cat)]^{+}$ couple; 2, V(V/IV) couple; 3, V(IV/III) couple; and 4, oxidation of the catecholato ligands.

The results of CV studies (Figure 2) were used to design the conditions for the bulk electrolysis experiments (Figure 3) and for the electrochemical XAS studies (Figures 4 and 5). Unlike for the previously studied Cr(V/IV/III) triscatecholato species, where all three oxidation states could be generated starting from $[Cr(cat)_3]^{3-}$,[13] the use of V complexes with at least two different catecholato ligands was required for the preparative generation of V(V), V(IV), and V(III) complexes. For all the bulk electrolysis experiments shown in Figure 3, the cell current dropped to <10% of the initial value within 30 min of bulk electrolysis (at 22 °C), and the results of coulometric measurements were consistent (within 10% experimental error) with one-electron oxidations or reductions of the complexes. Oxidation of $[Cr^{III}(tren)(cat)]^{+}$ in DMF solution at +600 mV (vs Ag/AgCl) led to a color change from blue to yellow-green. The UV−vis spectrum of the oxidation product (Figure 3a) possessed a sharp, intense signal at ~450 nm and smaller signals at ~580 and ~670 nm, consistent with a Cr(III) semiquinonato(1−) complex.[16,42] No such signals were observed for the one- and two-electron oxidation products of $[Cr^{III}(cat)_3]^{3-}$; instead, two broad absorption bands of similar intensity at ~500 and ~800 nm appeared for both products (Figure 3b).[13,42] These

Table 1. Typical Results of Cyclic Voltammetry for Cr and V Catecholato Complexes

couple[a]	$E_{1/2}$[b] (mV) vs Ag/AgCl	$E_{1/2}$[b] (mV) vs Fc^+/Fc^0	ΔE_p[c] (mV)	i_{pc}/i_{pa}[d]	solvent
$[Cr^{III}(tren)(sq)]^{2+}/[Cr^{III}(tren)(cat)]^+$	+368	−167	65	0.87	DMF
$[Cr^{IV}(cat)_3]^{2-}/[Cr^{III}(cat)_3]^{3-}$ [e]	−296	−831	60	0.95	DMF
$[Cr^{V}(cat)_3]^{-}/[Cr^{IV}(cat)_3]^{2-}$ [e]	−89	−624	63	1.1	DMF
$[Cr^{III}(sq)_3]^{0}/[Cr^{V}(cat)_3]^{-}$ [e]	+396	−139	61	1.0	DMF
$[V^{IV}(tcc)_3]^{2-}/[V^{III}(tcc)_3]^{3-}$	−581	−1088	80	1.1	MeCN
$[V^{V}(cat)_3]^{-}/[V^{IV}(cat)_3]^{2-}$	+76	−431	92	0.85	MeCN
$[V^{V}(dtbc)_3]^{-}/[V^{IV}(dtbc)_3]^{-}$	−270	−777	135	0.96	MeCN

[a] The corresponding cyclic voltammograms are shown in Figure 1 (scan rate, 100 mV s^{-1}; 100% *iR* compensation). [b] Half-wave potentials. [c] Separation of cathodic and anodic peaks. [d] Ratio of maximal cathodic and anodic currents. [e] Data from ref 13.

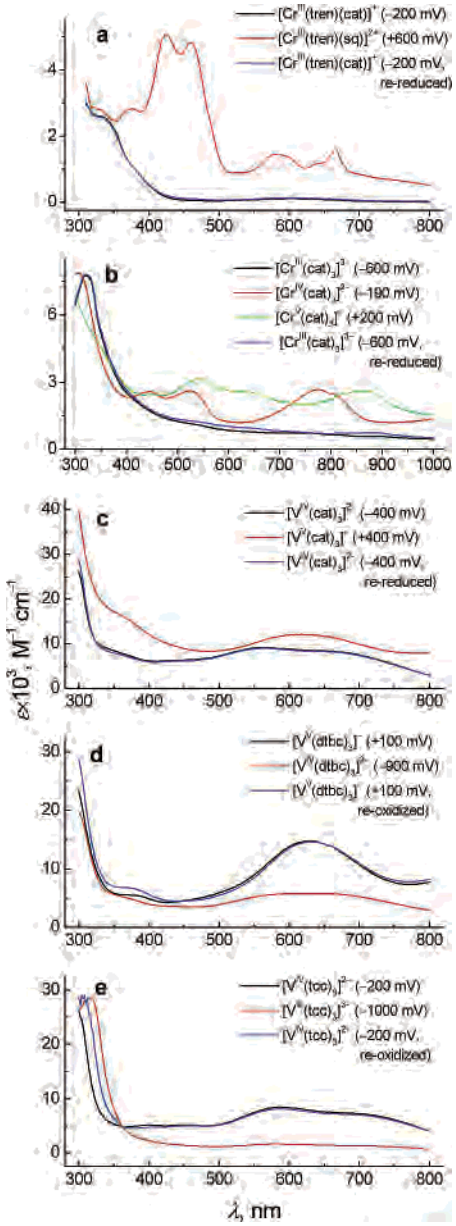

Figure 3. Typical changes in UV−vis spectra during the bulk electrolysis of Cr or V catecholato complexes (10 mM) in DMF (a and b) or MeCN (c−e) solutions in the presence of $(^nBu_4N)BF_4$ (0.10 M) and the corresponding catechols (20 mM, b−d only) at 22 °C. Samples of the reaction solutions (30 μL) were diluted 100-fold with the corresponding solvent (Ar-saturated). The values of the applied potentials are vs a Ag/AgCl reference electrode. Data in (b) are adapted from ref 13.

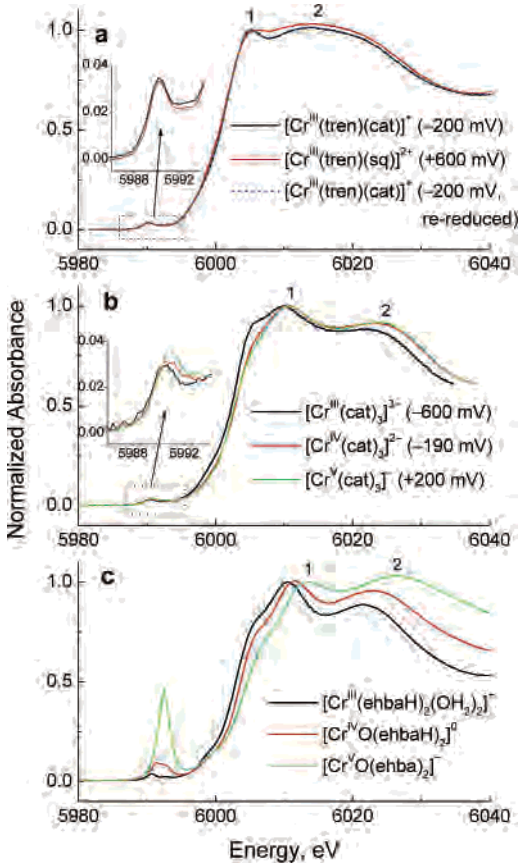

Figure 4. Typical XANES spectra of Cr(V/IV/III) complexes: (a) solutions generated by bulk electrolysis of $[Cr(tren)(cat)]^+$ (10 mM) in DMF at 22 °C; (b) solutions generated by bulk electrolysis of $[Cr(cat)_3]^{3-}$ (10 mM) in DMF in the presence of $catH_2$ (20 mM) at 22 °C (adapted from ref 13); and (c) frozen solutions of Cr(V/IV/III)−ehba complexes (10 mM) in H_2O at 10 K (adapted from ref 35). Bulk electrolysis for (a) and (b) was performed in the presence of $(^nBu_4N)BF_4$ (0.10 M) as the supporting electrolyte. The values of the applied potentials are vs a Ag/AgCl reference electrode.

bands are similar to those observed in the V(V/IV) complexes. Oxidation of $[V^{IV}(cat)_3]^{2-}$ (MeCN solution, +400 mV vs Ag/AgCl) led to a color change from dark purple to ink-blue and to an increase in absorbance at ∼600 nm (Figure 3c), whereas an opposite process was observed during the reduction of $[V^{V}(dtbc)_3]^{-}$ (MeCN solution, −900 mV vs Ag/AgCl, Figure 3d). These changes are consistent with the formation of the corresponding V(V) or V(IV) complexes.[20] Reduction of $[V^{IV}(tcc)_3]^{2-}$ in MeCN solution at −1000 mV led to a color change from blue to green and to a decrease in absorbance intensity at 500−800 nm (Figure 3e), consis-

(42) Sofen, S. R.; Ware, D. C.; Cooper, S. R.; Raymond, K. N. *Inorg. Chem.* **1979**, *18*, 234−239.

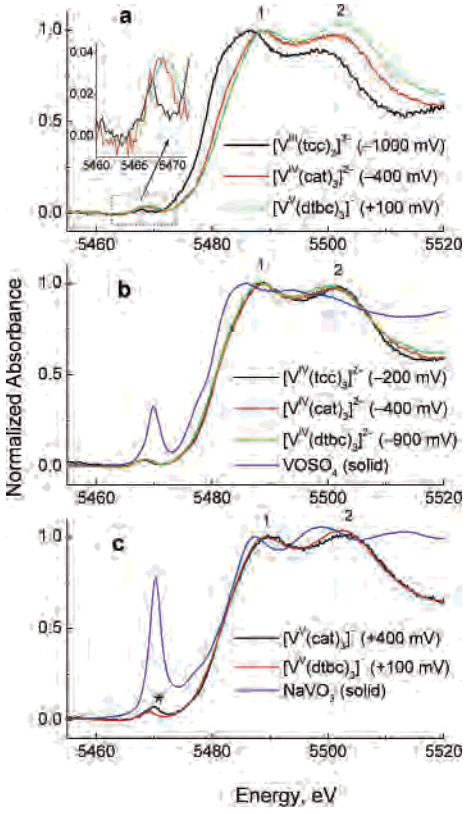

Figure 5. Typical XANES spectra of V(V/IV/III) triscatecholato complexes (10 mM), generated by bulk electrolysis in MeCN solutions in the presence of the corresponding catechols (20 mM) and (^{n}Bu$_4$N)BF$_4$ (0.10 M) at 22 °C, in comparison with those of typical V(V/IV) oxo complexes (solid mixtures of $VOSO_4 \cdot 5H_2O$ or $NaVO_3$ with BN, 22 °C). The values of the applied potentials are vs a Ag/AgCl reference electrode. An increased pre-edge absorbance for $[V^V(cat)_3]^-$ (indicated with an asterisk in part c) is probably due to the presence of traces of V(V) oxo complexes.

tent with the formation of a V(III) complex.[20] In all cases, reoxidation or re-reduction of the bulk electrolysis products led to the UV−vis spectra that were close to those of the original complexes (Figure 3a−e). In addition, the integrities of the $[V^{IV}(cat)_3]^{2-}$, $[V^{IV}(dtbc)_3]^{2-}$, and $[V^{IV}(tcc)_3]^{2-}$ species in solutions generated by bulk electrolysis were confirmed by EPR spectroscopy (Figure S4 in the Supporting Information). The EPR spectral parameters observed for these solutions ($g_{iso} \approx 1.950$, $A_{iso}(^{51}V) \approx 7.5 \times 10^{-3}$ cm^{-1}, Figure S4 in the Supporting Information) were characteristic for V(IV) triscatecholato complexes,[43] whereas typical V(IV) oxo complexes (such as $[V^{IV}O(acac)_2]$ or $[V^{IV}O(OH_2)_5]^{2+}$, Figure S4 in the Supporting Information) possess significantly higher g_{iso} and A_{iso} values.[44,45]

Electrochemical XANES Spectroscopy. Changes in the XANES spectra during the in situ bulk electrolysis (at 22 °C) of $[Cr(tren)(cat)]^+$ and three V(V/IV) triscatecholato complexes are shown in Figures 4a and 5. For all the compounds studied, changes in the XANES spectra were fully reversible, as illustrated in Figure 4a. The XANES spectra of the following compounds are shown for comparison: (i) Cr(V/IV/III) triscatecholato complexes, generated by bulk electrolysis of $[Cr^{III}(cat)_3]^{3-}$ in DMF solutions (Figure 4b);[13] (ii) typical Cr(III), Cr(IV), and Cr(V) complexes with a redox-inert ligand (ehbaH$_2$ = 2-ethyl-2-hydroxybutanoic acid; Figure 4c);[35] and (iii) reference V(IV) and V(V) compounds, including $VOSO_4 \cdot 5H_2O$ (or $[VO(OH_2)_5](SO_4)$)[46] and $NaVO_3$ (Figure 5b,c). Characteristic parameters of all XANES spectra (Figures 4 and 5) are listed in Table S3 of the Supporting Information.

Oxidation of $[Cr^{III}(tren)(cat)]^+$ to $[Cr^{III}(tren)(sq)]^{2+}$ did not result in significant changes in the edge energy or in the pre-edge absorbance intensity (Figure 4a and the Supporting Information, Table S3), which suggested that the metal center remains in the Cr(III) oxidation state.[14,38] These results are in contrast with a small (0.5 eV) but reproducible increase in the edge energy during the one-electron oxidation of $[Cr^{III}(cat)_3]^{3-}$ and with the increases in pre-edge absorbance intensity during the two-step oxidation of $[Cr^{III}(cat)_3]^{3-}$ (Figure 4b), which point to increases in the effective oxidation states of Cr.[13] On the other hand, the differences in XANES spectra between various oxidation states of Cr triscatecholato complexes (Figure 4b) are much less pronounced than those for Cr(V/IV/III)−ehba complexes (Figure 4c), where changes in the oxidation states led to the appearance of an oxo group and to significant changes in the coordination geometry,[35] which also contributes to the larger differences in the series.

Changes in XANES spectra for V(V/IV/III) triscatecholato complexes (Figure 5a) were similar to those for the corresponding Cr(V/IV/III) complexes (Figure 4b), except for larger shifts in edge energies between oxidation states (e.g., 1.7 eV for V(IV/III) vs 0.5 eV for Cr(IV/III), Table S3 in the Supporting Information). The XANES spectral features of V(V/IV/III) complexes with various catecholato ligands were determined by the oxidation state of the metal rather than by the nature of the ligands, as illustrated by close matches of XANES spectra for the three V(IV) complexes studied (Figure 5b) or the two V(V) complexes (Figure 5c). The spectra in Figure 5a,b were also consistent with the previously reported XANES spectra of the solid $K_3[V^{III}(cat)_3]$ and $(Et_3NH)_2[V^{IV}(cat)_3]$ complexes.[9] The spectra of V(V/IV) triscatecholato complexes were clearly distinguished from those of typical V(V/IV) oxo complexes by their low pre-edge absorbances (Figure 5b,c, in agreement with the literature data),[9] similar to the differences between octahedral Cr(III) complexes and less-symmetrical Cr(V/IV) oxo complexes (illustrated in Figure 4c).[35]

Notably, all the increases in the oxidation states of Cr or V complexes, shown in Figures 4 and 5, were accompanied by increases in the intensities of second vs first postedge peaks (designated as 2 and 1 in Figures 4 and 5; the corresponding ratios are given in Table S3 of the Supporting Information), even if the oxidation state of the metal was not changed (as in Figure 4a). This feature may be useful in the diagnostics of the oxidation states of metal ions in biological or environmental samples.[9,47]

(43) Branca, M.; Micera, G.; Dessi, A.; Sanna, D.; Raymond, K. N. *Inorg. Chem.* **1990**, *29*, 1586−1589.
(44) Farrell, R. P.; Lay, P. A. *Appl. Magn. Res.* **1996**, *11*, 509−519.
(45) Howes, B. D.; Kühlmeyer, C.; Pogni, R.; Basosi, R. *Magn. Res. Chem.* **1999**, *37*, 538−544.
(46) Francavilla, J.; Chasteen, N. D. *Inorg. Chem.* **1975**, *14*, 2860−2862.

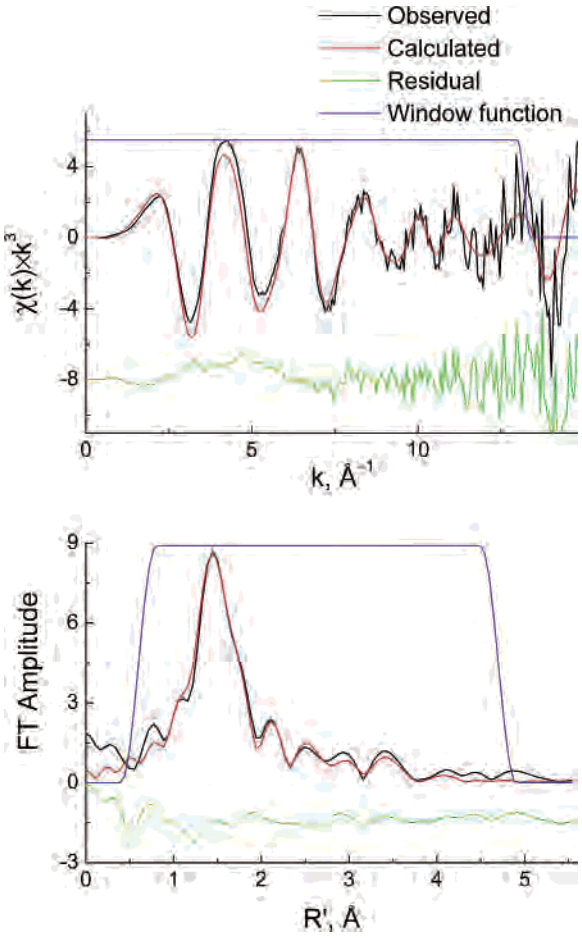

Figure 6. Observed and calculated XAFS and FT XAFS spectra of $[Cr^{III}(tren)(cat)]^+$ (10 mM solution in DMF; 0.10 M $(^nBu_4N)BF_4$; applied potential, −200 mV vs Ag/AgCl; 22 °C). Details of XAFS calculations are given in Tables S4−S6 of the Supporting Information.

Electrochemical XAFS Spectroscopy. Typical observed and calculated XAFS and Fourier transform (FT) of the XAFS spectra for Cr and V catecholato complexes are illustrated in Figure 6. The rest of the spectra, as well as detailed results of MS XAFS modeling, are given in the Supporting Information, Figures S5−S12 and Tables S4−S9. The optimized values of M−O bond lengths (M = Cr or V), as well as those for the previously studied Cr triscatecholato complexes,[13] are listed in Table 2. All the structural parameters of Cr and V catecholato complexes, obtained by MS fits to the XAFS (see the Supporting Information, Tables S5 and S8), were consistent with the available crystallographic information (a comparison of M−O bond lengths obtained by both methods is shown in Table 2).[2,4,16,20,41]

As for the previous studies on Cr(V/IV/III) triscatecholato complexes,[13] systematic errors in the bond lengths, obtained by MS XAFS fittings, were determined from the effect of deviations (with respect to the optimized values) in the bond lengths to the goodness-of-fit parameter (*R*). In each series of calculations, the lengths of one bond type (M−O, O−C, or C−C) were varied (by restraining them to a desired value within 0.002 Å), whereas the other bond lengths were restrained to the optimized values (within 0.002 Å; see the Supporting Information, Tables S5 and S8). The results for the M−O bond lengths (Figure 7) show that significant increases in the *R* value (≥0.5%) were caused by deviations from the optimum by ∼0.005 Å. Consistent with the previous results,[13] larger deviations in the C−O or C−C bond lengths (0.02−0.03 Å) were required to cause similar increases in *R* values. The usual conservative estimate of systematic errors in MS XAFS calculations of bond lengths is 0.01−0.02 Å.[14] The current results show that different values have to be applied, dependent on the type of scatterer and the absorber−scatterer distance. Random errors in the bond lengths, arising from the noise in the data (Monte Carlo analyses),[32] did not exceed 0.005 Å for the M−O bonds and 0.01 Å for the other coordination shells (see the Supporting Information, Tables S5 and S8).

The results of MS XAFS fittings (Table 2) show a small (∼0.01 Å, Figure 7) increase in the average Cr−O bond length caused by the oxidation of $[Cr^{III}(tren)(cat)_3]^+$ to $[Cr^{III}(tren)(sq)]^{2+}$, which is consistent with the crystallographic data for the related complexes with substituted catecholato ligands.[2,16] Notably, the MS XAFS fittings also reproduced decreases in the Cr−N and O−C bond lengths (by 0.02−0.03 and 0.08−0.10 Å, respectively; see the Supporting Information, Table S4) in $[Cr^{III}(tren)(sq)]^{2+}$ compared with $[Cr^{III}(tren)(cat)]^+$, observed in the crystal structures[2,16] (these values were not restrained during the MS XAFS calculations, see the Supporting Information, Table S4). Significant increases in the average V−O bond lengths within the V(V/IV/III) triscatecholato series (Table 2) were consistent with the crystallographic data for the corresponding complexes.[20,41] The optimized values of O−C and C−C bond lengths in the ligands (1.32(1) and 1.39(1) Å, respectively) were equal for all three oxidation states of V complexes (see the Supporting Information, Table S8). This feature, as well as the low values of Debye−Waller factors for the C and O atoms in the ligands (0.001−0.007 $Å^2$; see the Supporting Information, Table S8) are consistent with the presence of three equivalent catecholato ligands in V(V/IV/III) complexes. In the cat complexes, the shortening of the Cr−O bond length for the Cr(III) to Cr(IV) oxidation (∼0.04 Å) is somewhat smaller than the corresponding change in the V−O bond length (∼0.06 Å) in the tcc complexes. Similarly, the shortening of the Cr−O bond length for the Cr(IV) to Cr(V) oxidation (∼0.006 Å) is somewhat smaller than the corresponding change in the V−O bond length (∼0.025 Å) in cat complexes, but these changes are still significant given that there would be an increase in these values on oxidation if it was predominantly ligand-based.

Density Functional Calculations. In an effort to explain the differing redox behavior of the $[Cr(tren)(cat)]^{n+}$ ($n = 1$ or 2) and $[Cr(cat)_3]^{m-}$ ($m = 1-3$) series in terms of Cr−O bond lengths and Cr K-edge XANES spectra, we performed calculations of the geometric and electronic structures of the full range of oxidation states of these species. For a preliminary validation of the theoretical procedure that was used, we calculated the electronic structure of the unsubstituted semiquinonato ligand and compared it with the U-

(47) Gould, E. S. *Coord. Chem. Rev.* **1994**, *135*, 651−684.

Table 2. Typical Metal−Ligand (O) Bond Lengths in Cr and V Catecholato Complexes

			M−O (Å)		
complex	solvent[a]	E (mV)[a]	XAFS[b]	XRD[c]	DFT[d]
$[Cr^{III}(tren)(cat)]^{+}$	DMF	−200	1.912(5)	avg. 1.911(4)[e]	1.92, 1.89
$[Cr^{III}(tren)(sq)]^{2+}$	DMF	+600	1.920(5)	1.90−1.94[e]	1.95, 1.92
$[Cr^{III}(cat)_3]^{3-}$	DMF	−600	1.980(5)[f]	1.97−2.00[g]	2.04(0.1)
$[Cr^{IV}(cat)_3]^{2-}$	DMF	−190	1.943(5)[f]	1.94−1.96[h]	1.98(3)
$[Cr^{V}(cat)_3]^{-}$	DMF	+200	1.937(5)[f]	1.92−1.95[h]	1.94(0.1)
$[V^{III}(tcc)_3]^{3-}$	MeCN	−1000	2.012(5)	avg. 2.013(9)[i]	2.08(3)[l]
$[V^{IV}(cat)_3]^{2-}$	MeCN	−400	1.936(5)	avg. 1.942(8)[j]	1.99(0.1)
$[V^{IV}(dtbc)_3]^{2-}$	MeCN	−900	1.946(5)		
$[V^{IV}(tcc)_3]^{2-}$	MeCN	−200	1.948(5)		
$[V^{V}(cat)_3]^{-}$	MeCN	+400	1.911(5)		1.93(0.1)
$[V^{V}(dtbc)]^{-}$	MeCN	+100	1.912(5)	avg. 1.91(4)[k]	

[a] Conditions of bulk electrolysis used for generation of the corresponding complexes for XAS studies (22 °C, Figures 2 and 3). [b] Determined by MS fittings of XAFS spectra (Figures 6, and the Supporting Information Figures S5−S12 and Tables S4−S9). Errors in the last significant figures (given in parentheses) were determined by a combination of Monte Carlo analyses for the noise-related errors (see the Supporting Information, Tables S5 and S8) and analyses of the systematic errors (Figure 7). [c] X-ray crystallographic data (∼22 °C). [d] Results of DFT calculations, unrestricted BP, see text for details. Standard deviations ($\times 10^{-2}$) in the calculated distances (where there are more than two) are given in parentheses. [e] Data for the corresponding complexes with 3,6-di-*tert*-butyl-substituted catecholato ligands.[2,16] [f] Data from previous studies.[13] [g] Data for $K_3[Cr(cat)_3]$.[5b] [h] Data for the corresponding complexes with tetrachloro- or tetrabromo-substituted catecholato ligands.[4a] [i] Data for $K_3[V^{III}(cat)_3]$.[20,41] [j] Data for $(Et_3NH)_2[V^{IV}(cat)_3]\cdot CH_3CN$.[20,41] Similar bond lengths (1.93−1.97 Å) were found in the crystal structures of this compound at 150 K and $(Et_3NH)_2[V^{IV}(cat)_3]$ at 25 K (see CIF files in the Supporting Information). [k] Data for $Na[V^{V}(dtbc)_3]$.[41] [l] Calculated for a complex with the unsubstituted catecholato ligand.

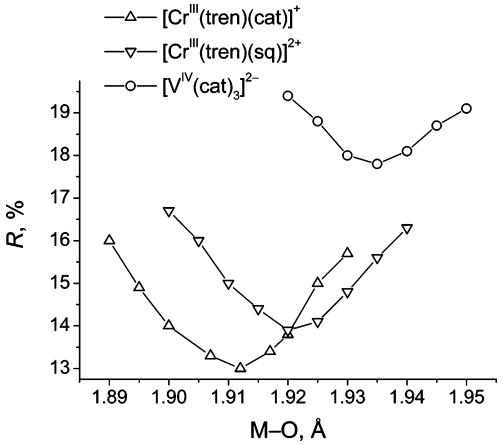

Figure 7. Typical examples for the influence of the changes in M−O (M = Cr or V) bond lengths on the goodness-of-fit parameters in MS XAFS calculations (see the Supporting Information, Tables S4−S9, for details).

BLYP results reported by Rodriguez et al.[2] for the di-*tert*-butyl-substituted ligand. The unrestricted BP calculations showed qualitatively identical electronic structure in terms of energetic ordering, symmetry, and composition of frontier orbitals (HOMO − 2, HOMO − 1, HOMO, and LUMO). The BP results showed a slightly smaller split of the occupied α and unoccupied β levels of the HOMO (0.544 vs 0.624 eV, between 61α and 61β from ref 2) and a slightly larger split between the α HOMO and α LUMO (3.273 vs 3.158 eV). The unrestricted BP-calculated electronic structure of the triplet state of $[Cr(tren)(3,6\text{-}dtbc)]^{2+}$ gave identical ordering and character of the frontier orbitals (HOMO − 4 through LUMO + 1) as the U-BLYP results,[2] but there is a reversal in the energetic ordering of HOMO − 5 and HOMO − 6. The calculated HOMO−LUMO gap was 0.865 eV, compared to the reported value of 0.801 eV.[2] The HOMO and HOMO − 1 values were calculated to be switched in energy between the complex (charge = 2+) with the substituted semiquinonato and that with the unsubstituted semiquinonato ligand. The HOMO for $[Cr(tren)(cat)]^{2+}$ is delocalized between the metal and the semiquinonate ligand and has β spin.

Table 2 shows calculated M−O bond lengths for the $[Cr(tren)(cat)]^{n+}$ and $[Cr(cat)_3]^{m-}$ series in comparison with experimentally determined values. In both cases, the trend in the experimental M−O bond lengths is matched by the theoretical results, i.e., increasing with oxidation for $[Cr(tren)(cat)]^{n+}$ and decreasing for $[Cr(cat)_3]^{m-}$; however, the magnitude of the trend is somewhat overestimated by the DF calculations, particularly for the triscatecholato species. A similar observation was made for the V(III/IV/V) series (Table 2). The calculated results reflect the well-known tendency of nonlocal density functional theory to overestimate metal-ligand bond distances, in this instance by as much as 0.07 Å. A larger spread of M−O distances was calculated for $[Cr^{IV}(cat)_3]^{2-}$ and for the isoelectronic $[V^{III}(cat)_3]^{3-}$ than for the other charge states.

Mulliken spin populations are also shown in Table 3. The calculated quartet state of $[Cr(tren)(cat)]^{+}$ has a great majority of the spin localized on the metal atom. Oxidation to $[Cr(tren)(sq)]^{2+}$ leaves the spin population on Cr unchanged but leads to an increase of 0.9 in β spin on what is now appropriately denoted the semiquinonato ligand, which gives rise to an antiferromagnetically coupled triplet state, consistent with that reported previously.[2] Examination of the metal-atom spin populations for the $[Cr(cat)_3]^{m-}$ and $[V(cat)_3]^{m-}$ series reveals that electrons are being lost from orbitals significantly delocalized between metal and ligands, with the extent of delocalization being greater for Cr than for V. For the $m = 3- \rightarrow 2-$ oxidation step, roughly two-thirds of an electron is lost from Cr, whereas for V, four-fifths of an electron is lost. For the $m = 2- \rightarrow 1-$ step, more electron density is lost from the ligands (55%) than from the Cr center (no information can be gained using this method for this step for V, as the oxidized form is a fully coupled singlet state). Nevertheless, the spread of the lost electron density over the three ligands means that they remain predominantly (∼70%) of catecholato nature (Table 3).

Table 3. Selected DFT Calculated Properties in Cr and V Catecholato Complexes

complex	Mulliken metal-atom partial charge	Mulliken metal-atom spin density	Mulliken ligand spin density	metal *d* orbital contribution to HOMO (%)
$[Cr^{III}(tren)(cat)]^{+}$	0.87	2.91	~0	11
$[Cr^{III}(tren)(sq)]^{2+}$	0.92	2.97	−0.90[a]	22
$[Cr^{III}(cat)_3]^{3-}$	0.90	2.98	~0	38
$[Cr^{IV}(cat)_3]^{2-}$	0.88	2.34	−0.34[b]	74
$[Cr^{V}(cat)_3]^{-}$	0.87	1.89	−0.89[b]	
$[V^{III}(cat)_3]^{3-}$	1.05	2.06	~0	73 (62)[c]
$[V^{IV}(cat)_3]^{2-}$	1.04	1.21	−0.21[b]	
$[V^{V}(cat)_3]^{-}$	1.04	0	0	

[a] Localized on the semiquinonato ligand. [b] Total density for the three catecholato ligands. [c] Value in parentheses is for the LUMO—equivalent to the HOMO of the Cr(III) complex.

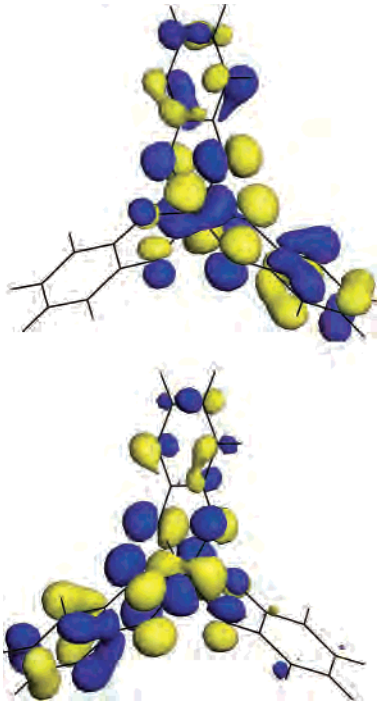

Figure 8. Three-dimensional isosurface plots of the single-electron (spin-unrestricted) HOMO (below) and HOMO-1 (above) for $[Cr(cat)_3]^{3-}$ determined at the BP/DNP level (see Experimental Section). Strong metal−ligand delocalization is noted and also occurs between two of the three ligands in each case. The predominant bonding nature of the orbitals is π-antibonding with respect to both Cr−O and C−O for one ligand in each case.

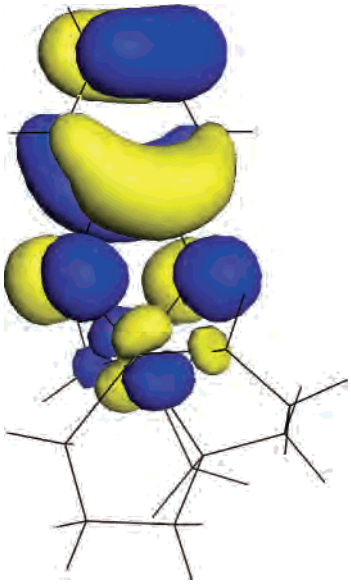

Figure 9. Three-dimensional isosurface plot for the single-electron (spin-unrestricted) HOMO of $[Cr(tren)(cat)]^{+}$ determined at the BP/DNP level (see Experimental Section). The predominant bonding nature of the orbital is π-antibonding with respect to both Cr−O and C−O for the catecholato ligand.

Figures 8 and 9 show isosurface plots for the calculated HOMO and HOMO − 1 of $[Cr(cat)_3]^{3-}$ and the HOMO of $[Cr(tren)(cat)]^{+}$, which are the orbitals mainly involved in the reversible redox processes identified above. These three orbitals are essentially similar in character, being π-antibonding with respect to both Cr−O and C−O (predominantly of one ligand for the HOMO of $[Cr(cat)_3]^{3-}$ and another ligand for the HOMO − 1).

Discussion

The metal catecholato systems studied previously[13] and in this work represent three possible classes of redox couples: (i) the predominantly ligand-based reactions for the $[Cr^{III}(tren)(cat)]^{+}/[Cr^{III}(tren)(sq)]^{2+}$ couple; (ii) the both metal- and ligand-based reactions with strong electron delocalization between the metal ion and the ligands for Cr(V/IV/III) triscatecholato complexes; and (iii) the predominantly metal-based reactions for V(V/IV/III) triscatecholato complexes. The differences between these systems are reflected most clearly in the M−O bond lengths (M = Cr or V) for different oxidation states of the complexes. An increase in the average Cr−O bond length in $[Cr^{III}(tren)(sq)]^{2+}$ compared with that of $[Cr^{III}(tren)(cat)]^{+}$ (1.920(5) vs 1.912(5) Å, Table 2 and Figure 7) is consistent with a decrease in the donor ability of a semiquinonato(1−) ligand compared with that of a catecholato(2−) ligand.[2,13] In both the Cr and V triscatecholato systems, the M−O bond lengths decreased significantly when the oxidation states of the complexes increased (consistent with the increases in the effective oxidation states of the metal ion),[15] but the magnitudes of these changes for the Cr complexes (1.980(5), 1.943(5), and 1.937(5) Å, Table 2)[13] were smaller than the corresponding values for the V complexes (e.g., 2.012(5), 1.948(5), and 1.912(4) Å at 22 °C, Table 2). Whereas the changes in the bond lengths for the second oxidation step for the Cr series are within experimental error, the errors are expected to be in the same direction for all complexes and, hence, this difference is probably real. The differences in the trends in bond lengths are also consistent with a smaller magnitude of changes in the edge energies in XANES spectra

of the Cr(V/IV/III) triscatecholato complexes compared with those of the V(V/IV/III) complexes (Figures 4b and 5a and the Supporting Information, Table S3). By contrast, XANES spectra of the Cr(III)-tren-cat(sq) complexes indicated the absence of significant changes in the oxidation state of Cr (Figure 4a and Table S3). A strong pre-edge XANES peak, which is commonly used as an indicator of the formation of Cr(IV/V) species and is due to a reduction in symmetry at the Cr center that results in increased mixing of the ligand p orbitals (particularly for oxo ligands) into metal d orbitals, is not observed here, as the complexes retain octahedral symmetry throughout.

Additional evidence for the different oxidation mechanisms in Cr(III) mono- and triscatecholato complexes was obtained from electronic absorption spectroscopy of the oxidation products (Figure 3). The intensity of the charge-transfer band of $[Cr(tren)(sq)]^{2+}$ ($\lambda = 420-460$ nm, $\epsilon = (4.8-5.1) \times 10^3$ M^{-1} cm^{-1}, Figure 3a) was roughly three times lower than the corresponding value ($\lambda_{max} \approx 520$ nm, $\epsilon_{max} \approx 12 \times 10^3$ M^{-1} cm^{-1}) for the $[Cr^{III}(dtbsq)_3]$ complex (dtbsq = 3,5-di-*tert*-butyl-1,2-semiquinonato(1−)).[42] This feature confirms the existence of a correlation between the number of semiquinonato ligands in the complex and the intensity of the 400−500 nm absorbance band. If the one- and two-electron oxidations of $[Cr^{III}(cat)_3]^{3-}$ were ligand-centered (i.e., led to $[Cr^{III}(cat)_2(sq)]^{2-}$ and $[Cr^{III}(cat)(sq)_2]^{-}$, respectively),[1,4] the intensity of the 400−500 nm band for $[Cr^{III}(cat)(sq)_2]^{-}$ would be roughly twice as high as that for $[Cr^{III}(cat)_2(sq)]^{2-}$ or $[Cr^{III}(tren)(sq)]^{2+}$, which is not observed experimentally (Figure 3a,b). Instead, the broad absorbance bands of similar intensity at 400−600 and 700−900 nm, observed for the oxidation products of $[Cr^{III}(cat)_3]^{3-}$, are consistent with the spectra of typical Cr(IV) and Cr(V) complexes.[47,48] Moreover, these bands are similar to the broad bands observed in the V(V) and V(IV) complexes (Figure 3c−e), where there is little dispute as to the spectroscopic metal oxidation state. It is clear, however, that further oxidation of the Cr(V) complex results in complete ligand oxidation to form $[Cr^{III}(dtbsq)_3]$. Not only is this deduced from the electronic absorption spectroscopy but it is also consistent with a shift of the XANES edge energy back to that of Cr(III) and a lengthening of the Cr−O bond lengths, as we reported previously.[13] The data on the neutral $[Cr(cat)_3]$ complex will not be discussed further because it was too unstable under the conditions of the spectroelectrochemistry to record accurate XAFS data for multiple-scattering analysis.

On an empirical level, different mechanisms of redox reactions for the Cr mono- and triscatecholato systems can be correlated to the differences in their redox potentials (Table 1). The strong σ- and π-donor properties of catecholato ligands compared with the tren ligand shift the redox potential of the Cr(IV/III) couple to more negative values, so the oxidation of $[Cr^{III}(cat)_3]^{3-}$ occurs predominantly at the metal ion, whereas that for $[Cr^{III}(tren)(cat)]^{+}$ is ligand-centered.

Mulliken spin populations (Table 3) provide a much more reliable predictor of the spectroscopic oxidation state of metal centers in these complexes, which indicates predominantly metal-based oxidations with increasing ligand-based character, for $[V(cat)_3]^{3-}$ to $[V(cat)_3]^{2-}$, $[Cr(cat)_3]^{3-}$ to $[Cr(cat)_3]^{2-}$, and $[Cr(cat)_3]^{2-}$ to $[Cr(cat)_3]^{-}$, respectively, with the latter showing roughly equal metal- versus ligand-based character. Clearly, electron density is being lost from the HOMO, with significant contribution from the metal center in each case (see Figure 8 and Table 3). The trend in the variation of the spin populations on oxidation of the $[Cr(cat)_3]^{n-}$ series (decreasing α spin on the metal, increasing β spin on the ligands) is similar to that calculated for the $[V(cat)_3]^{n-}$ series, which is widely accepted in the literature as undergoing metal-based oxidation; however, the trend is clearly distinct from that of the tren complex (invariant α spin on the metal, increasing β spin on the ligand), which is widely accepted as undergoing ligand-based oxidation. This supports our assertion that the $[Cr(cat)_3]^{n-}$ series undergoes predominantly metal-based oxidation.

The reason for the difference in behavior with respect to the Cr−O distances between the triscatecholato and tren-monocatecholato complexes is also evident from the calculations. In both cases, the orbitals from which electrons are removed on oxidation are antibonding with respect to both Cr−O and catecholato C−O bonds. In the absence of redox-active ligands, this would clearly lead to a contraction of Cr−O bond distances on oxidation; however, the partial oxidation of the ligand toward a semiquinonato donor generates a weaker σ-donor ligand and acts to lengthen the Cr−O distance. For $[Cr(tren)(cat)]^{+}$, the strong σ-donor tren ligand lowers the energy of the Cr *d* orbitals such that they do not interact strongly with the catecholato ligand, which is reflected in the low Cr contribution to the HOMO of this complex (Table 3). This effect results in a mainly ligand-based HOMO and oxidation and subsequent lengthening of the Cr−O bonds. By contrast, for the triscatecholato series, in the absence of the tren ligand, the catecholato moiety does interact strongly with the Cr, leading to a HOMO with significantly higher metal character and resulting in a contraction of the Cr−O bonds on oxidation. The Cr−O lengthening effect due to partial oxidation of the ligand is further minimized by the fact that the HOMO is spread over more than one ligand.

In summary, the results of this work support the earlier suggestion[11,13] that Cr(IV) and Cr(V) complexes, stabilized by electron delocalization between the Cr ion and the ligands, are formed during the oxidation of Cr(III) triscatecholato complexes or during the reduction of Cr(VI) by catechols (in a large molar excess). Recently, new evidence for the ability of catecholato ligands to stabilize high oxidation states of Cr was obtained in the studies of the reactions of $[Cr^0(CO)_6]$ or $[Cr^{III}(acac)_3]$ with 3,6-di-*tert*-butyl-*o*-benzoquinone in polymer matrices, where the formation of Cr(IV) and Cr(V) species was detected by IR and EPR spectroscopies, respectively.[49] Stabilization of the Cr(IV) oxidation state in polymer matrixes is particularly promising for use in laser devices.[49] On the other hand, stabilization of Cr(V) and Cr-

(48) Farrell, R. P.; Lay, P. A. *Comments Inorg. Chem.* **1992**, *13*, 133−175.

(IV) species by biological ligands, such as catecholamines, is likely to contribute to the toxicity and carcinogenicity of Cr compounds.[8,50]

Acknowledgment. Financial support of this work was provided by an Australian Research Council (ARC) grant, an ARC Professorial Fellowship, and the Australian Synchrotron Research Program (ASRP) grant for access to the ANBF facility (to P.A.L.); an ASRP Postdoctoral Fellowship to H.H.H.; an ARC RIEFP grant for the fluorescence detector at ANBF; and ARC and Wellcome equipment grants for the EPR instrumentation. The ASRP is funded by the Commonwealth of Australia under the Major National Research Facilities Program. We thank Dr. Peter Barnard and Mr. Jack Zylmans (University of Sydney) for assistance in the design and construction of the electrochemical XAS cell, and Professor Leo Radom (University of Sydney) for discussions regarding the theoretical component of this work.

Supporting Information Available: Experimental details on the synthesis and characterization of the complexes; figures showing the typical ESMS and FTIR data for the synthesized complexes, EPR spectra of V(IV) triscatecholato complexes in solutions, the atomic numbering used in the MS XAFS calculations, and observed and calculated XAFS spectra of Cr and V catecholato complexes; tables showing the summary of crystallographic data for $(Et_3NH)_2[V^{IV}(cat)_3]$ at 25 K and $(Et_3NH)_2[V^{IV}(cat)_3]\cdot CH_3CN$ at 150 K (CIF files), and the assignment of major ESMS signals and details of MS XAFS calculations. This material is available free of charge via the Internet at http://pubs.acs.org.

IC0603611

(49) Rakhimov, R. R.; Hwang, J. S.; Prokof'ev, A. I.; Alexandrov, I. A.; Zelenetskii, A. N.; Aleksandrov, A. I. *J. Appl. Phys.* **2004**, *95*, 7342−7344.

(50) Levina, A.; Codd, R.; Dillon, C. T.; Lay, P. A. *Prog. Inorg. Chem.* **2003**, *51*, 145−250 and references therein.